2007

Influence of Sea Ice Cover and Icebergs on Circulation and Water Mass Formation in a Numerical Circulation Model of the Ross Sea, Antarctica

Michael S. Dinniman
Old Dominion University, msd@ccpo.odu.edu

John M. Klinck
Old Dominion University, jklinck@odu.edu

Walker O. Smith

Influence of sea ice cover and icebergs on circulation and water mass formation in a numerical circulation model of the Ross Sea, Antarctica

Michael S. Dinniman,[1] John M. Klinck,[1] and Walker O. Smith Jr.[2]

[1] Satellite imagery shows that there was substantial variability in the sea ice extent in the Ross Sea during 2001–2003. Much of this variability is thought to be due to several large icebergs that moved through the area during that period. The effects of these changes in sea ice on circulation and water mass distributions are investigated with a numerical general circulation model. It would be difficult to simulate the highly variable sea ice from 2001 to 2003 with a dynamic sea ice model since much of the variability was due to the floating icebergs. Here, sea ice concentration is specified from satellite observations. To examine the effects of changes in sea ice due to iceberg C-19, simulations were performed using either climatological ice concentrations or the observed ice for that period. The heat balance around the Ross Sea Polynya (RSP) shows that the dominant term in the surface heat budget is the net exchange with the atmosphere, but advection of oceanic warm water is also important. The area average annual basal melt rate beneath the Ross Ice Shelf is reduced by 12% in the observed sea ice simulation. The observed sea ice simulation also creates more High-Salinity Shelf Water. Another simulation was performed with observed sea ice and a fixed iceberg representing B-15A. There is reduced advection of warm surface water during summer from the RSP into McMurdo Sound due to B-15A, but a much stronger reduction is due to the late opening of the RSP in early 2003 because of C-19.

1. Introduction

[2] There have been dramatic interannual changes in the sea ice cover over parts of the Ross Sea in recent years. In coastal seas around Antarctica, much of the interannual variability in the observed sea ice has been postulated to be a result of large-scale environmental effects such as the Antarctic Circumpolar Wave [*White and Peterson*, 1996], the multidecadal warming in the Antarctic Peninsula [*Vaughan et al.*, 2003], ENSO [*Yuan and Martinson*, 2000], and the Southern Annular Mode [*Hall and Visbeck*, 2002]. In the Ross Sea however, much of the recent (2000–2004) variability in sea ice extent is thought to be due to several large icebergs that have calved off the Ross Ice Shelf and moved through the area [*Arrigo and van Dijken*, 2003]. In March 2000 the iceberg B-15 was formed and a large fragment, B-15A ($\approx$6400 km^2 in surface area and 160 km

long), grounded near the east end of Ross Island in January 2001. Another smaller iceberg (C-16) that had been dislodged from the ice shelf by B-15 had previously grounded along Ross Island in November 2000. These two icebergs remained at their respective locations (Figure 1) until October 2003 when B-15A began to break up. Throughout the period when both icebergs were grounded, substantial changes were observed in ice concentration and distribution in the Ross Sea. Presumably, ocean circulation, primary production, and other aspects of the coastal ecosystem were altered as well [*Arrigo et al.*, 2002; *Smith et al.*, 2006]. In May 2002 the iceberg C-19 ($\approx$32 km wide and 200 km long) calved off the Ross Ice Shelf and started drifting northward. Between December 2002 and February 2003, C-19 rotated in place near Pennell Bank (Figure 2) and by April had begun to move northward out of the Ross Sea. Satellite imagery shows that during the austral summer of 2002–2003 there was unusually high ice cover in the southwestern Ross Sea, and this was likely due at least in part to the restricted advection of sea ice away from the Ross Ice Shelf due to the presence of C-19 [*Arrigo and van Dijken*, 2003].

[3] Several different water masses (using definitions from *Carmack* [1977] and repeated by *Jacobs and Giulivi*

[1]Center for Coastal Physical Oceanography, Old Dominion University, Norfolk, Virginia, USA.
[2]Virginia Institute of Marine Science, College of William and Mary, Gloucester Point, Virginia, USA.
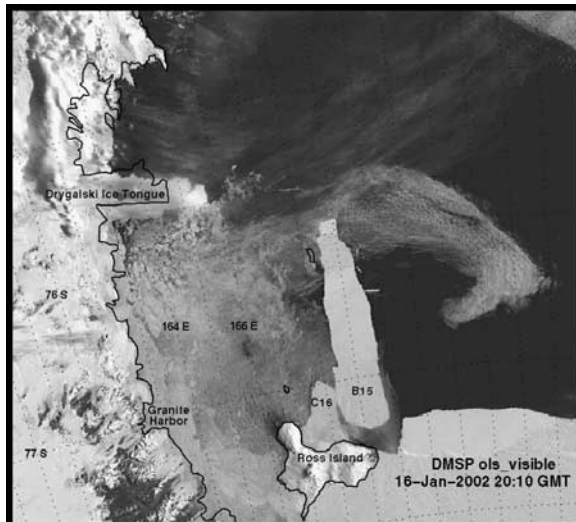
Figure 1. DMSP satellite image showing Ross Island, iceberg B-15A and iceberg C-16 on 16 January 2002. Image courtesy Raytheon Polar Services.

1999]) can be found on the continental shelf in the Ross Sea. Ice Shelf Water (ISW) has temperatures below the surface freezing point and is created by water in contact with the ice shelf at depth. Subfreezing temperatures occur because the in situ freezing temperature in seawater decreases with increasing pressure. This water emerges from beneath the Ross Ice Shelf primarily in the west-central part of the continental shelf. High-Salinity Shelf Water (HSSW) is very dense water often defined by salinities greater than 34.6 psu and temperatures at or near the surface freezing point. HSSW is found in the southwestern Ross Sea and is formed by brine release in coastal polynyas on the shelf [*Jacobs and Giulivi*, 1998; *VanWoert*, 1999]. Export of this water from the shelf is thought to be important in the formation of Antarctic Bottom Water [*Jacobs et al.*, 1985; *Orsi et al.*, 1999; *Gordon et al.*, 2004]. Circumpolar Deep Water (CDW) is a relatively warm, salty, and nutrient-rich water mass, originally created in the North Atlantic, that is the most voluminous water mass of the Southern Ocean. At the shelf break, CDW flows onto the continental shelf at middepth through episodic but persistent intrusions at specific locations due to bottom topography [*Dinniman et al.*, 2003]. This water mixes on the shelf to become modified CDW (MCDW), which has temperatures of 1.0 to $-1.5°C$, is an important source of heat and nutrients onto the continental shelf [*Budillon et al.*, 2000; *Dinniman et al.*, 2003] and has important effects on several different physical (including ice cover [*Jacobs and Comiso*, 1989; *Fichefet and Goosse*, 1999]) and biological (such as productivity [*Peloquin and Smith*, 2007]) processes.

[4] Large icebergs could have a number of effects on ocean and sea ice conditions. The most obvious is a blocking effect on the motion of sea ice. A more subtle blocking effect is due to the strong control of topography on circulation which would change subsurface water motion and affect heat, salt, and other advective fluxes. Two mixing effects are produced by a large iceberg. Relative motion of the ice and water create turbulence which would lead to mixing in the wake of the iceberg. If the iceberg is thick enough to penetrate the permanent pycnocline, then deep melting on the berg could produce a secondary circulation, similar to that created by an ice shelf, which would provide a vertical transport of water and associated properties.

[5] It would be difficult to accurately simulate the highly variable sea ice concentrations from 2001 to 2003 with just a dynamic sea ice model since much of the variability was due to the effects of the icebergs in the area. However, a model with imposed sea ice and icebergs could be used to study the oceanic response. In this study a high-resolution (5 km) primitive equation general circulation model of the Ross Sea (including the cavity underneath the Ross Ice Shelf) is used to examine the effects of the icebergs and sea ice on the circulation and water masses in the Ross Sea. We found that the large icebergs had significant effects on oceanic circulation on the continental shelf.

2. Methods

[6] The Ross Sea circulation model is based on the Rutgers/UCLA Regional Ocean Model System (ROMS) [*Shchepetkin and McWilliams*, 2005]. This model is similar to the one described by *Dinniman et al.* [2003]; only the major features and differences from the previous model will be discussed here. The primary difference is that the model domain has been extended southward to include the water-filled cavity beneath the Ross Ice Shelf (RIS). The model domain (Figure 3) extends from well north (67.5°S) of the continental shelf break southward to 85°S, which includes almost all of the cavity beneath the RIS. The horizontal grid spacing is 5 km and there are 24 vertical levels whose thickness varies with the water column depth but are concentrated towards the top and bottom surfaces. For example, for a typical shelf water column thickness of 500 m, the top layer is 4.97 m thick, the bottom layer is 6.32 m thick, and the maximum thickness in the middle is 40.47 m.

[7] Two bathymetric surfaces must be defined for this model: the bottom of the water column and, where necessary, the draft below mean sea level of the ice shelf (Figure 4). Both of these were obtained from the BEDMAP gridded digital model of ice thickness and subglacial topography for Antarctica [*Lythe et al.*, 2001]. The sea floor topography in the BEDMAP model is derived from the *Smith and Sandwell* [1997] ETOPO2 global 2 min
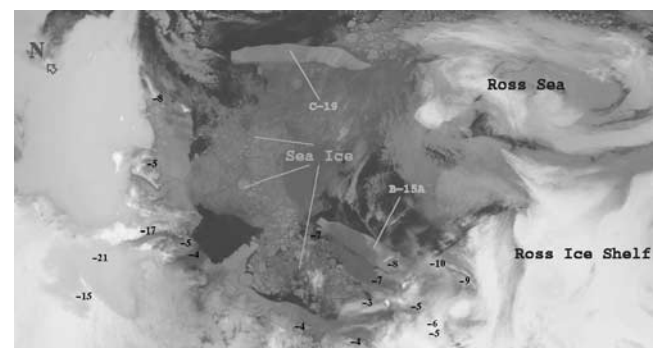

Figure 2. Satellite image showing icebergs B-15A and C-19 on 16 January 2003. The numbers represent Automated Weather Station air temperatures (°C). Image courtesy of AMRC-University of Wisconsin.
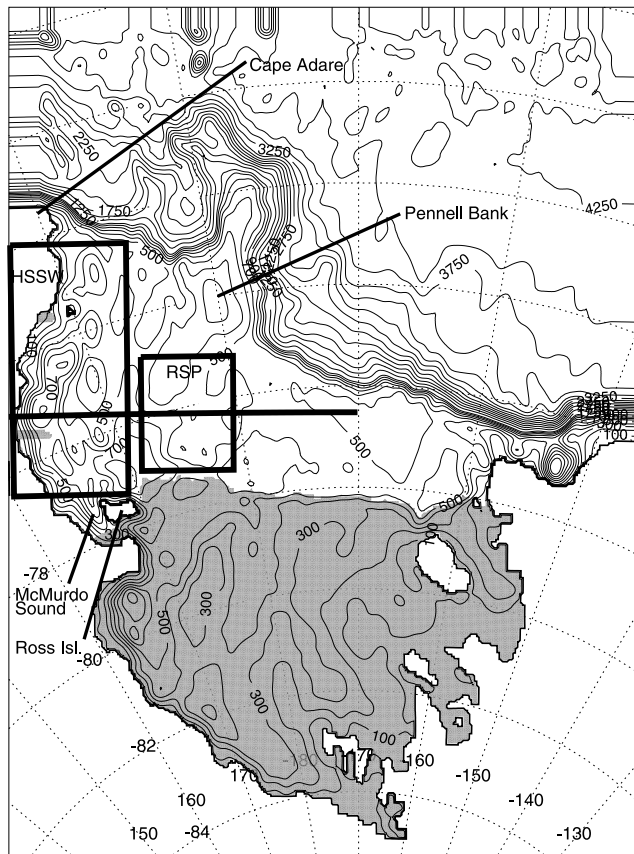
Figure 3. Domain for the Ross Sea Model. The contour interval for the bathymetry is 100 m up to 1000 m depth and 250 m deeper than 1000 m. The shaded areas represent the extent of the ice shelf. The contours below the ice shelf represent water column thickness. The box labeled RSP represents an area around the Ross Sea Polynya that will be discussed in section 3.1.2. The box labeled HSSW represents an area of HSSW formation in the western Ross Sea that will be discussed in section 3.1.4. The horizontal line represents the cross section in Figure 5.

resolution bathymetry and (south of 72°S) the 1/12° ETOPO5 bathymetry [*National Geophysical Data Center* (NGDC), 1988]. Both surfaces were slightly smoothed with a modified Shapiro filter which was designed to selectively smooth areas where the changes in the ice thickness or bottom bathymetry are large with respect to the total depth [*Wilkin and Hedström*, 1998]. The position of the RIS front was forced to remain constant during the smoothing.

[8] Initial fields of temperature and salinity are computed from the World Ocean Atlas 2001 (WOA01), and the values in the Ross Sea just north of the RIS are extrapolated southward to represent the initial conditions underneath the RIS. Open boundaries for all runs are handled as in the work of *Dinniman et al.* [2003] except that the temperature and salinity used for the adaptive nudging on the boundaries is now from WOA01. Vertical momentum and tracer mixing were handled using the K profile parameterization (KPP) mixing scheme [*Large et al.*, 1994] with the small changes for sea ice given by *Dinniman et al.* [2003]. Daily values of wind stress and wind speed were

obtained from a blend of QuikSCAT scatterometer data and NCEP analyses [*Milliff et al.*, 2004] to give a repeatable cycle over a 2 year (a) (2000 and 2001) period. The blended winds are distributed on a 1/2° grid. However, there is very little scatterometer data in the blended winds in our area and the effective wind resolution is that of the underlying NCEP analyses (about 2.0°).

2.1. Sea Ice and Open Water

[9] In place of a fully dynamic sea ice model, ice concentrations from a climatology derived from the Special Sensor Microwave Imager (SSM/I) are imposed. The model surface heat flux is calculated as a linear combination of heat flux due to ice cover and the open water heat flux with the ratio determined by the ice concentration in that grid cell [*Markus*, 1999]. The open water heat flux was calculated with the COARE version 2.0 bulk flux algorithm [*Fairall et al.*, 1996] with most of the necessary atmospheric data coming from monthly climatologies from either the ECMWF (ERA-40) reanalysis (air pressure, humidity, and air temperature) or the ISCCP cloud climatology. Daily winds were used for the open water heat flux calculation. The shortwave solar radiation was computed using the model of *Zillman* [1972] with the cloud cover correction algorithm of *Antoine et al.* [1996] and an assumed oceanic albedo of 0.10. The model surface fresh water flux (imposed as a salt flux) is also calculated as a linear combination of open water evaporation minus precipitation and that due to ice melting or freezing [*Markus*, 1999]. The frazil ice term contribution to the salt flux in the work of *Markus* [1999] that was removed from the calculation in the work of *Dinniman et al.* [2003] has been restored but only when the temperature in the top layer is below the surface freezing point. This was important in simulating the high salinities on the far western continental shelf. The only relaxation term in the surface forcing was a very weak (relaxation timescale of 3 a) restoration of the surface salinity to the monthly WOA01 values. Additional details are given by *Dinniman et al.* [2003].
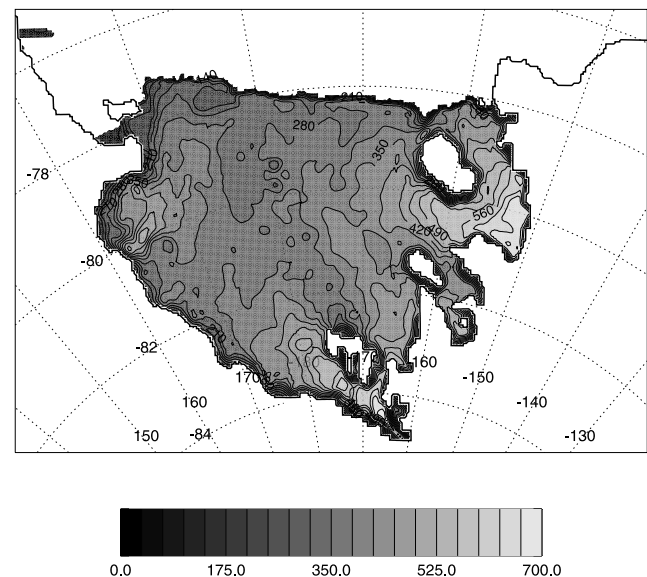

Figure 4. Model ice shelf draft below mean sea level (m).

Table 1. Constants in Ice Shelf Flux Equations

Parameter	Value
ρ_i (ice density)	930 kg m^{-3}
L (latent heat of fusion)	3.34×10^5 J kg^{-1}
c_{pi} (specific heat capacity of ice)	2000 J (kg °C)$^{-1}$
c_{pw} (specific heat capacity of sea water at 0°C)	4000 J (kg °C)$^{-1}$
γ_T (turbulent exchange coefficient for heat)	10^{-4} m s^{-1} [Hellmer and Olbers, 1989]
γ_S (turbulent exchange coefficient for salt)	5.05×10^{-7} m s^{-1} [Hellmer and Olbers, 1989]

2.2. Ice Shelf

[10] The thickness and extent of the ice shelf do not change over the time covered by the model. Under the ice, the upper boundary of the model is no longer at sea level but conforms to the ice shelf base. The pressure gradient force calculation [Shchepetkin and McWilliams, 2003] accounts for the possibility that the top surface of the water may have a significant slope due to the ice shelf. The hydrostatic pressure at the base of the ice shelf is computed by assuming that the ice is in isostatic equilibrium. This pressure can be calculated by the integral over depth (from mean sea level to the base of the ice shelf) of the density of the water replaced by the ice. Instead of assuming that the density in the integral can be approximated by the density at the first level of the ocean model directly beneath the ice [e.g., Grosfeld et al., 1997] or a constant average density for every location [e.g., Beckmann et al., 1999], the density at the first level of the ocean model [$\rho(top)$] minus an assumed constant linear dependence of the density with depth ($\partial\rho/\partial z$) is used to give a pressure of:

$$P = g\left(\rho(top) - 0.5\frac{\partial\rho}{\partial z}H_i\right)H_i \qquad (1)$$

where g is the gravitational acceleration and H_i is the ice shelf draft. The change in density with pressure for water near freezing and salinities in the range 34.0–35.0 psu is relatively constant for the first few hundred meters from the surface and an average over this range ($\partial\rho/\partial z = 4.78 \times 10^{-3}$ kg m^{-4}) was used.

[11] Below the ice shelf the atmospheric contributions to the momentum and buoyancy flux are set to zero. Friction between the ice shelf and the water is computed as a quadratic stress with a coefficient of 3.0×10^{-3} (nondimensional) and is applied as a body force over the top three ocean levels.

[12] At the ocean-ice shelf interface, a parameterization with a viscous sublayer model is used with three equations representing the conservation of heat, the conservation of salt and a linearized version of the freezing point of sea water as a function of salinity and pressure. The free variables are T_b, which is the temperature at the ice shelf base, S_b, which is the salinity at the ice shelf base, and $\frac{\partial h}{\partial t}$, which is the melting (<0) or freezing (>0) rate (m s^{-1}).

$$\rho_i\left(L - c_{pi}\Delta T\right)\frac{\partial h}{\partial t} = \rho c_{pw}\gamma_T(T_b - T_w) \qquad (2)$$

[13] Equation (2) represents the conservation of heat across the ocean-ice shelf boundary where ρ_i is the average ice density (Table 1), L is the latent heat of fusion, c_{pi} is the specific heat capacity of ice, ΔT is the temperature difference between the ice shelf interior (assumed to be the minimum of −1.95°C or the air temperature above the ice shelf) and the freezing temperature at the ice shelf base (set here to be −1.95°C), ρ is density of the water in the mixed layer, c_{pw} is the heat capacity of sea water at 0°C, γ_T is the turbulent exchange coefficient for heat and is chosen to be a constant and T_w is the water temperature in the uppermost grid box.

$$\rho_i S_b \frac{\partial h}{\partial t} = \rho\gamma_s(S_b - S_w) \qquad (3)$$

[14] Equation (3) represents the conservation of salt across the ocean-ice shelf boundary where γ_S is the turbulent exchange coefficient for salt and is also chosen to be a constant and S_w is the salinity in the uppermost grid box.

$$T_b = 0.0939 - 0.057S_b + 7.6410 \times 10^{-4}h \qquad (4)$$

[15] Equation (4) is a linearized version of the equation for the freezing point of sea water [Foldvik and Kvinge, 1974], where h is the depth below mean sea level.

[16] These equations can be solved simultaneously (using known mixed layer and ice properties) to calculate heat and freshwater (salt) fluxes into the ocean [Hellmer et al., 1998; Holland and Jenkins, 1999]. This has been done previously for several simulations of the flow beneath ice shelves [e.g., Beckmann et al., 1999; Timmermann et al., 2002; Holland et al., 2003]. The calculation of the actual heat and salt fluxes into the top model layer of the ocean includes the "meltwater advection" terms for boundary conditions through a material surface that can be important in long simulations or with high basal melt rates [Jenkins et al., 2001].

2.3. Experiments

[17] A spinup simulation starting in late austral winter (15 September) was run for 6 a. Three experiments (Table 2) were then performed to examine the effects of the differences in the sea ice and the icebergs. In the first (the "CLMICE" simulation), the base simulation was continued (including using monthly climatological sea ice) but with daily wind speed and wind stress covering the time 15 September 2001 to 15 September 2003. The second experiment (the "VAR-ICE" simulation) is forced by the same winds as CLMICE but with imposed sea ice from the observed monthly concentration for the period September 2001 to September 2003. The final experiment ("ICEBERG") uses the VARICE forcing with one large iceberg in the location and with the approximate combined area and volume of icebergs B-15A and C-16. This simulation also ran for 2 a (15 September 2001 to 15 September 2003).

[18] The iceberg is simply implemented in the model as another fixed ice shelf and is not advected into position over time. Experimental radar soundings of B-15A give an estimated range of thickness along the centerline of 200–270 m [Blankenship et al., 2002]. In the model, ice of constant draft (220 m) is imposed just east of Ross Island to

Table 2. Model Experiments

Experiment	Conditions
CLMICE	Climatological sea ice, No B-15A
VARICE	Time varying sea ice (9/2001–9/2003), No B-15A
ICEBERG	Time varying sea ice (9/2001–9/2003), B-15A

match the extent of B-15A and C-16, while another area of ice is removed from the ice shelf to represent the condition after iceberg C-19 calved. In grid cells where ice was added, the temperature and salinity surfaces from the spinup that are below the depth of the ice are reinterpolated vertically onto the new layer depths. In grid cells where ice was removed, the temperature and salinity in the new water "created" are initialized to be a constant mixed layer extrapolated upward from the third layer from the top of the spinup. The iceberg is only grounded laterally in the model, but there are locations underneath the iceberg where the water column is reduced by as much as 81%.

3. Results
3.1. Effects of Climatological Versus Observed Ice Cover
3.1.1. Comparison of CLMICE Run to Observations

[19] Since there is no surface temperature relaxation in the model, comparing the model sea-surface temperature (SST) to satellite observations serves as a check on several processes, including open-water surface heat flux, heat transfer between the ice and the water, penetration of the solar heating below the surface, horizontal advection, and vertical mixing. This comparison was performed by *Dinniman et al.* [2003] but is recalculated due to the changes in the model. As before, a climatology of Advanced Very High Resolution Radiometer (AVHRR) satellite SST covering 1985–2000 averaged over 5-d periods [*Casey and Cornillon*, 1999] is interpolated onto the model grid and compared to model SST. Note though that there can be problems with the AVHRR Pathfinder SST at high latitudes [*Podestá et al.*, 2003]. A climatology of model SST was created from the 2 a of the CLMICE run. The model climatology was compared with the satellite climatology every 10 d at every grid point where AVHRR data are available (low or no sea ice) for the time period when AVHRR data are available for more than 90% of the non-ice-shelf model domain (late November through mid-March). The timing of the SST annual cycle in the model matches very well with observations. The average rms error for the model climatology over this period is 0.36°C with a maximum of 0.46°C in late January. The errors over the model grid are mostly compensated at any given time with only a small warm bias over the period of 0.20°C.

[20] Cross sections of salinity (Figure 5) in summer and early spring from 170°W to the coast from the CLMICE simulation show the seasonal cycle of HSSW formation in the southwestern part of the Ross Sea. A comparison with an observed cross section of salinity taken in February 1984 (not shown) [see *Jacobs and Giulivi*, 1999, Figure 4b] shows good agreement with the highest salinity waters in the west and the middepth salinity contours (34.5 and 34.6)

being similar. There are some noticeable differences, with the principal one being that the model results are not quite salty enough in the deep trench against the coast of Victoria Land. Also, the shallow surface layer of fresh water in the model from 170°W to about 180°E is not observed, although this could be due to local conditions when the observations were made. However, the model appears to be doing a reasonable job of creating HSSW on the shelf.

[21] An earlier model study [*Dinniman et al.*, 2003] examined the dynamics of the intrusion of warm, salty CDW onto the shelf, but it is now possible to help validate the locations of the modeled intrusions with a high-resolution (5 km) annual climatology of temperature and salinity that has recently been developed for the Ross Sea [*Stover*, 2006]. The mean temperature at 300 m for the CLMICE simulation (Figure 6) shows two primary locations along the shelf break where warm oceanic water intrudes onto the shelf at middepths: around Pennell Bank and a large region near 170°W. There are also two smaller regions in the model near 174°E and 160°W. While some of the details of the intrusions differ from the climatology, the mean locations of all four areas in the model match very well with the observed climatology. This shows that the model is also doing a reasonable job of simulating the intrusion of warm MCDW onto the shelf.

3.1.2. Ross Sea Polynya Heat Balance

[22] The Ross Sea Polynya is an area of reduced ice concentration surrounded by higher ice concentrations that is located along the Ross Ice Shelf. This polynya has an average area of 27,000 km^2 and is the largest polynya to regularly form around Antarctica [*Zwally et al.*, 1985; *Gloersen et al.*, 1992]. It usually becomes ice free in the early austral spring and then expands northward until it reaches the northern ice margin in January. The low sea ice
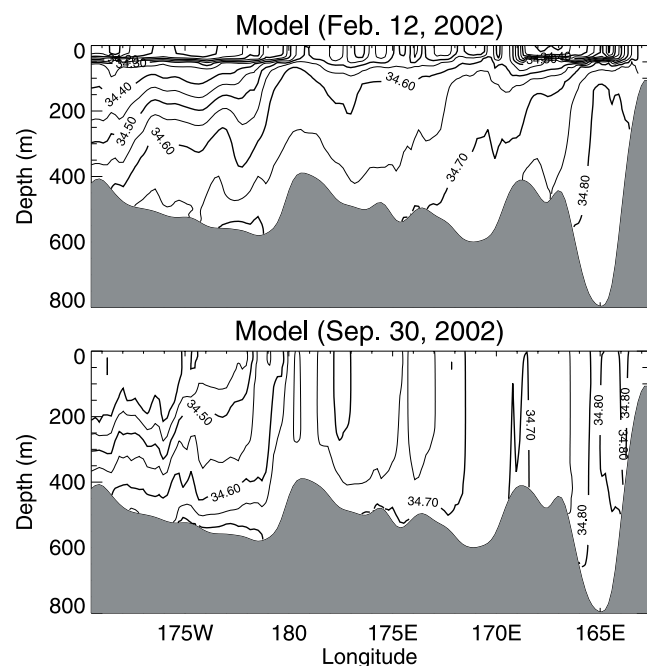

Figure 5. Cross section (see Figure 3) looking southward of model salinity (psu) in summer and early spring of 2002 for the CLMICE simulation.
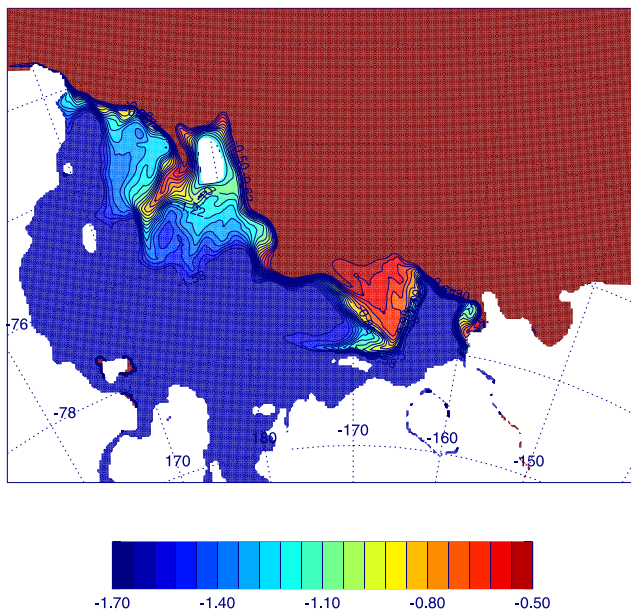
Figure 6. Average model temperature (°C) at 300 m for the CLMICE case. Note that the temperature scale is set so as to emphasize the intrusions of warm oceanic water onto the shelf.

in the polynya has been attributed to many processes, including southerly katabatic winds [*Bromwich et al.*, 1998], upwelling of warm CDW [*Jacobs and Comiso*, 1989], and combinations of the above [e.g., *Fichefet and Goosse*, 1999].

[23] Since this model imposes the sea ice, it is difficult to compute explicitly the relative importance of wind effects versus upwelling of warm water on the maintenance of the polynya. However, since the proper structure of the polynya is imposed, the SST's match observations, and we feel that at least some of the dynamics of the CDW intrusions are correct, it is instructive to look at the heat budget in the area.

[24] A heat budget (Figure 7) of the top 200 m of the water column for an area around the Ross Sea Polynya (Figure 3) for the VARICE simulation shows that during the summer of 2001–2002, the surface heat exchange is the predominant term in heating the water in early summer and cooling the water in the later part of the summer. However, even during the summer, the advection of heat into the area (which is always greater than zero) makes a contribution. Starting in April 2002, vertical diffusion of heat from below also brings a significant amount of heat into the upper water column. During the fall and winter, the total heat into the area is approximately zero with the surface loss terms balanced by the advection and diffusion of heat into the area. The following summer (2002–2003) had significantly more sea ice in the area of the RSP (22,500 km^2 in the defined area in mid-January versus a climatological value of 2000 km^2). This excessive sea ice led to much less surface and overall heating and thus advection of warmer water becomes a significant contributor to the heat budget even in summer. While the surface term was dramatically different in the heavy ice year and the vertical diffusion term (which depends on the temperature of the surface water) was

somewhat different, the advection term was not significantly affected by the difference in sea ice.

[25] Without a dynamic sea ice model, we cannot state what causes the surface heating term (which is strongly dependent on the imposed sea ice) to behave the way it does. The surface terms are the largest contributor to the summer heat budget. However, the advection and vertical diffusion of heat into the polynya area is an important part of the heat budget in the upper water column. Much of the heat that is diffused and advected from below (and a small portion of the heat that is advected laterally) is supplied to the shelf waters at depth through intrusions of CDW [*Dinniman et al.*, 2003], lending support to the idea that upwelling of relatively warm CDW does play some role in the appearance and maintenance of the Ross Sea Polynya.

3.1.3. Ice Shelf Basal Melting

[26] A two-dimensional picture (Figure 8) of the annual average basal melting for the second year of the CLMICE case shows the greatest melting primarily along the ice front and the northwestern edge of the cavity where warm surface waters flow into the cavity. There are also several locations of significant melting deep in the cavity mostly near the grounding line where the ice is very thick (Figure 4). Most of the freezing areas are in the central part of the ice shelf. The spatial pattern of the melting in the second year (not shown) of the VARICE simulation is very similar to the
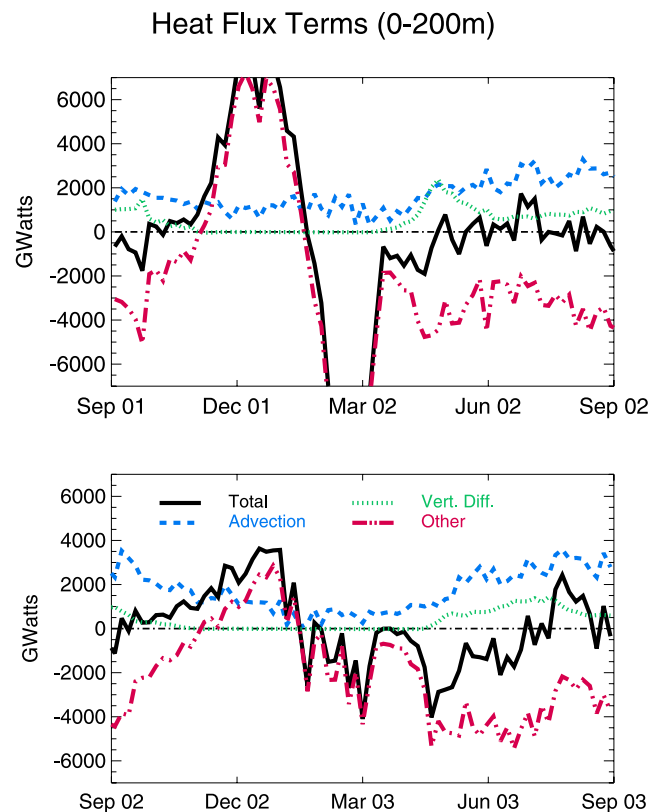
Heat Flux Terms (0-200m)

Figure 7. Heat flux term balance for the top 200 m of the water column in the RSP box in Figure 3 for the VARICE case. The "Other" term is the "Total" term minus the advection and vertical diffusion terms and is primarily surface heating/cooling.
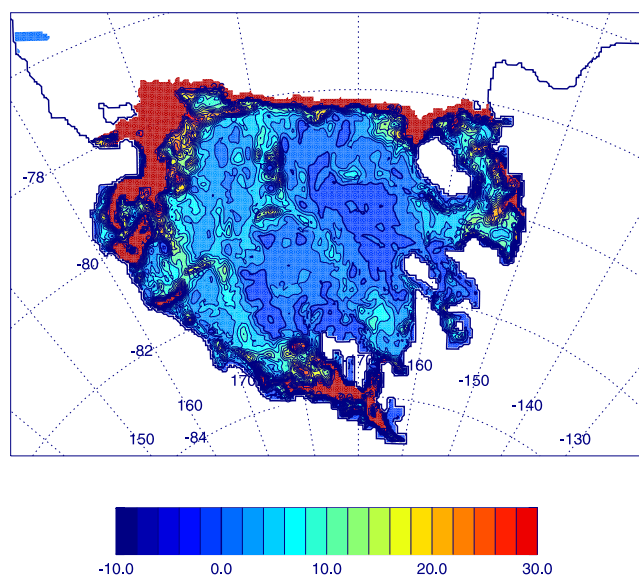
Figure 8. Annual basal melt rate (cm a^{-1}) September 2002 to September 2003 for the CLMICE simulation.

CLMICE case, except for some weaker melting just south of Ross Island.

[27] The average melt rate over the entire base of the Ross Ice Shelf has a seasonal cycle with increased melting during the austral summer in both the VARICE and CLMICE simulations (Figure 9). However, the higher ice cover during the summer of 2002–2003 in the VARICE case produces smaller basal melting in summer because there is less warm surface water to advect underneath the shelf. The annual average melt rate over both years of the CLMICE case is 14.2 cm a^{-1} while it is reduced to 13.4 cm a^{-1} for VARICE. For just the second year of the simulation, the annual average melt rate for the CLMICE case is 14.8 cm a^{-1} and is reduced to 13.0 cm a^{-1} for VARICE. Both of these are at the low end of the range (12–22 cm a^{-1}) of estimates for the area-average basal melt rate for the RIS [*Shabtaie and Bentley*, 1987; *Lingle et al.*, 1991; *Jacobs et al.*, 1992]. The difference in basal melt leads to small but noticeable differences in the mean water temperature in the northern part of the ice cavity and the volume of supercooled (colder than the surface freezing point) water in the non-ice-shelf covered McMurdo Sound area. There is not much difference between the two simulations in the volume of ISW over the entire open shelf. However, the simulations only ran for a few months past the summer of 2002–2003 and this may not be long enough to show differences in ISW creation and export to the shelf.

3.1.4. HSSW Formation

[28] The volume-averaged salinity below 200 m for an area (Figure 3) in the western Ross Sea for the two simulations shows (Figure 10) a seasonal cycle of about 0.016 psu for the CLMICE simulation with only a slight reduction (0.002 psu/a) in the mean annual salinity. The annual average salinity below 200 m of the entire open shelf only decreases by 0.001 psu/a. Note that *Jacobs et al.* [2002] do estimate an average decrease of 0.003 psu/a in the western Ross Sea from 1963 to 2000. The small interannual variability for the CLMICE case is to be

expected as all forcing except the wind is climatological. The strength of the annual cycle seems low when compared to observations at a single point in the area (e.g., the 0.08 psu range at 402 m and 0.04 psu range at 748 m measured in Terra Nova Bay from February to December 1995 [*Manzella et al.*, 1999]). However, the average is over a large (1.13 × 10^5 km^2) area. The seasonal cycle of the volume averaged mean salinity below 200 m for one model point in Terra Nova Bay for the CLMICE simulation (not shown) is 0.081 psu.

[29] The average salinity for the VARICE case starts to increase with respect to the CLMICE salinity in winter 2002. The difference rapidly increases to 0.012 psu by November 2002 and then stays about the same through March 2003. From March 2003 to the end of the simulations the difference slowly increases to 0.017 psu and then decreases to about 0.014 psu.

[30] The processes responsible for the difference in the area average salinity are shown by the differences between the two cases for each term in the salinity flux equation (Figure 11). Below 200 m the most important process is advection. Vertical diffusion (which includes winter convection) is almost the same in both simulations except during June to September 2002, where it is greater for the VARICE simulation. The salinity increase in the area of HSSW formation in the model during late 2002 is primarily due to advection from outside the area, but the vertical diffusion of salt does play a role. Since the only difference between the two simulations is the imposed sea ice, and the
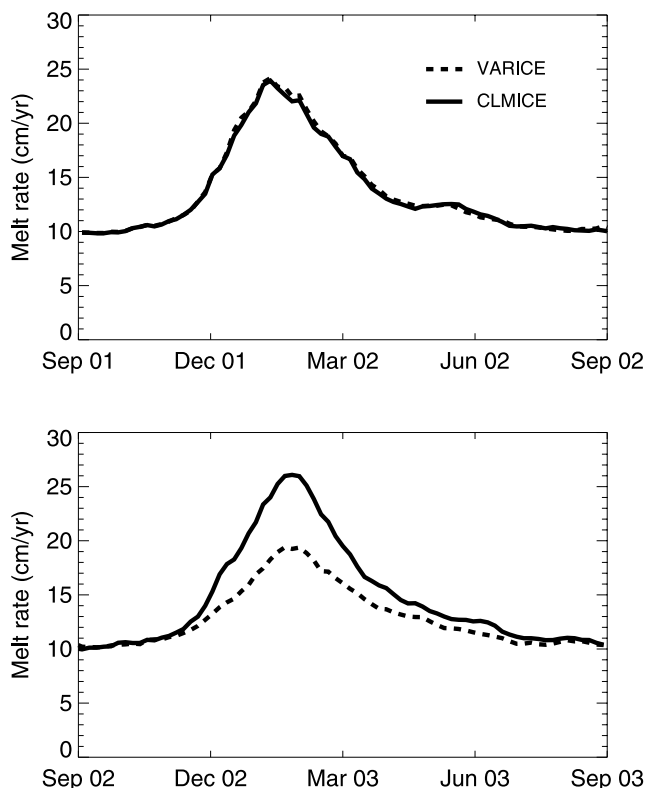
Avg. Basal Melt Rate

Figure 9. Time history of the average basal melt rate (cm a^{-1}) over the entire base of the Ross Ice Shelf.
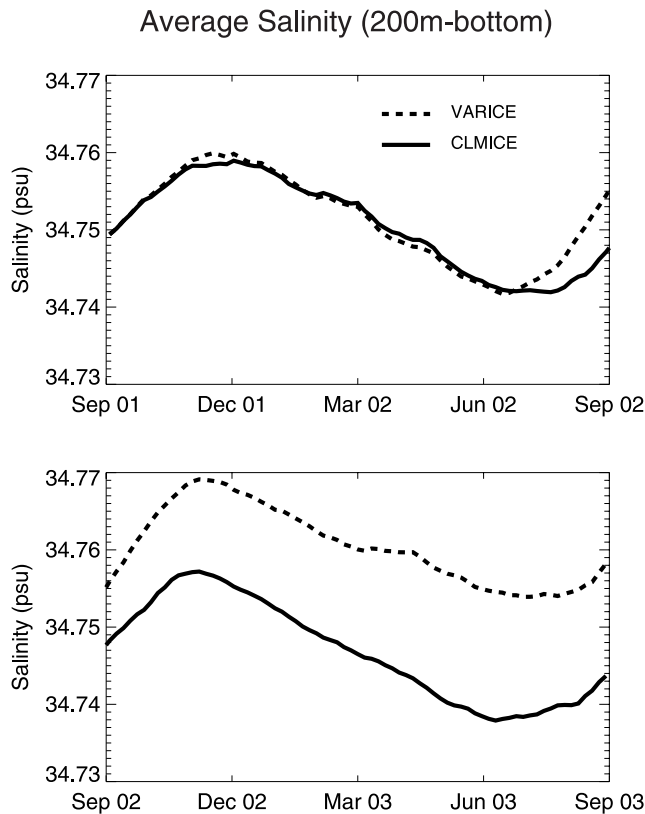
Average Salinity (200m-bottom)

Figure 10. Average salinity (psu) below 200 m for the area defined by the HSSW box in Figure 3.

resultant changes in the surface salinity flux, the sea ice must be the cause of the extra salt advected from outside the area. The difference in surface salt flux over the defined area between the two simulations (not shown) shows an increased surface salt flux (or reduced fresh water flux) for the VARICE simulation at several times from September 2001 through April 2002. This relative increase in salinity is "stored" in the surface mixed layer until the convection is strong enough to mix this water below 200 m.

[31] Thus the interannual difference in the imposed sea ice does have a noticeable effect on the high salinity shelf water formation in the western Ross Sea, although the sea ice directly above the formation region is not necessarily the most important contributor to the interannual changes in salinity in the deeper water. However, the great difference in the ice concentration in the austral summer of 2002–2003 did not have a large effect on the HSSW creation in the model.

3.2. Influence of Iceberg B-15A

[32] An important feature of the long-term mean subtidal flow in McMurdo Sound is the current from the open Ross Sea north of Ross Island entering the east side of the sound and flowing southward [*Heath*, 1977]. This water is typically warmer than the resident water and during austral summer this heat transport contributes to the consistent early season ice breakout observed in the east [*Heath*, 1977; *Mitchell and Bye*, 1985]. Part of the southward flow continues underneath the ice shelf south of Ross Island (McMurdo Ice Shelf); the rest is deflected westward around

the sound and northward along the western boundary. Supercooled water from underneath the ice shelf also contributes to the northern flow on the west side of the sound [*Heath*, 1977; *Lewis and Perkin*, 1985]. Currents in the center of the sound are less well known, but there are indications of southerly flow that is greater at depth [*Heath*, 1977], "mixed but slightly northward" flow [*Barry and Dayton*, 1988] or currents that result from a large anticyclonic eddy in the eastern part of the sound [*Lewis and Perkin*, 1985].

[33] The circulation in both the VARICE and CLMICE simulations matches the estimated average circulation. The summer surface circulation near Ross Island is somewhat variable due to strongly varying winds in the area. However, the mean summer surface circulation near Ross Island for the CLMICE simulation (Figure 12) has water from north of Ross Island turning southward into the eastern part of McMurdo Sound. Some of this flow continues under the ice shelf and then turns eastward south of Ross Island. There is also a return flow along the western edge of the sound that continues northward along Victoria Land. A northwestward current underneath the ice shelf contributes very cold water to the western side of the sound. The southward current in the central part of the sound may not be realistic, but the observations there are uncertain and this flow does not seem to have a large impact on the advection
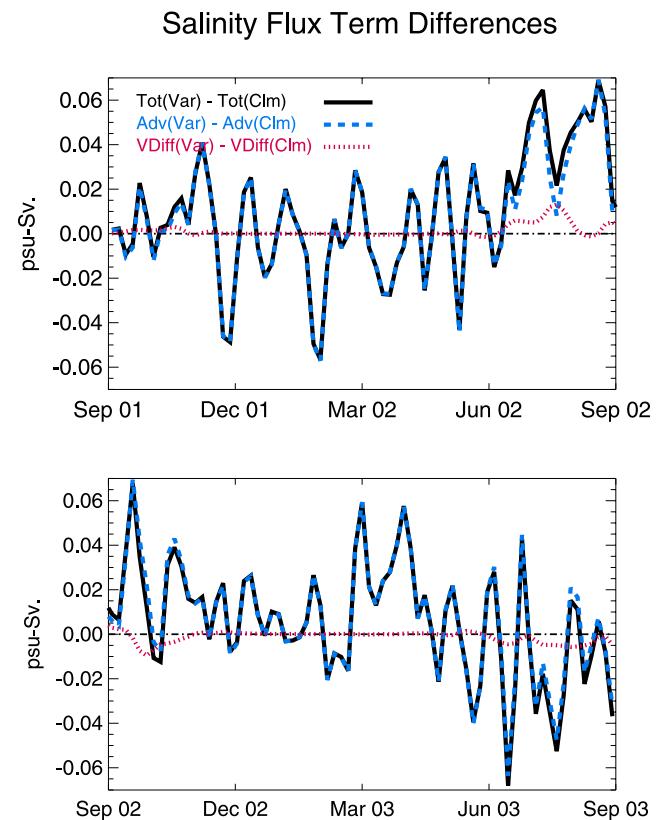
Salinity Flux Term Differences

Figure 11. Difference in salinity flux balance terms between the VARICE and CLMICE simulations for the volume below 200 m in the area defined by the HSSW box in Figure 3. Note that one pass of a 1-2-1 smoother has been applied to each difference term.
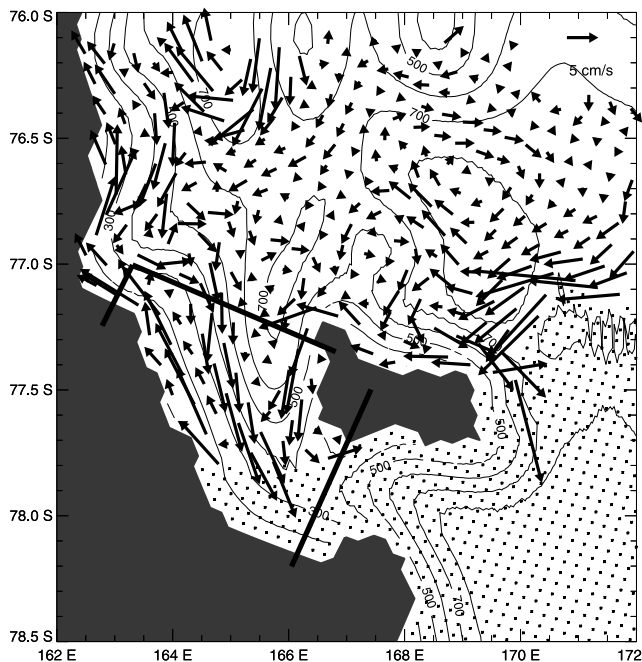
Figure 12. Model circulation at 20 m averaged over January and February for both years for the CLMICE case. The box represents the area over which the averages in Figures 15 and 16 are calculated. Black areas are land masked points and dotted areas represent ice shelf covered water points.

of warm water from the Ross Sea Polynya into the eastern sound (see below).

[34] There is little stratification below the surface mixed layer, and therefore much of the flow in the model is barotropic and follows the bathymetry. As a result, changes in water column thickness lead to circulation changes. In the ICEBERG simulation, the iceberg north of Ross Island partially blocks the westward flow of water from just north of the ice shelf. The summer surface circulation (Figure 13) still shows a current entering the eastern part of McMurdo Sound from north of Ross Island. However, this current is weaker now and the water in it follows a much different path and is further removed from the waters just north of the ice shelf.

[35] Climatologies of satellite SST observations [see *Dinniman et al.*, 2003, Figure 6b], show that the surface water north of Ross Island in summer is generally warmer to the east in the Ross Sea polynya. In mid-January 2003 in the CLMICE simulation, strong flow advects relatively warm surface waters into the eastern side of the sound (Figure 14a). The temperature in McMurdo Sound is slightly cooler for the ICEBERG case (Figure 14b) than the VARICE case (Figure 15), suggesting that advection of heat from the open Ross Sea into McMurdo Sound has been reduced by the grounded icebergs. Note that the imposed sea ice cover used to calculate the surface fluxes over the sound is the same for these two simulations which isolates the advective effects as the primary driver of the difference in the temperature in the sound. However, both the VARICE

case and the ICEBERG case are much cooler than the CLMICE case (Figure 14). The average temperature of the top 50 m of the water in McMurdo Sound during austral summer of 2002–2003 (Figure 15) shows that while the VARICE case is only slightly warmer than the ICEBERG case, the CLMICE case is significantly warmer than both. Of course, much of the higher temperature for the CLMICE case is due to the lower ice concentration that is directly imposed over the Sound. However, external effects are also important in determining the difference in temperature between the cases. A heat flux term balance calculation for the region shows that the advective heat flux (Figure 16) into the area in summer is greatest for the CLMICE case and only slightly larger for the VARICE case compared to the ICEBERG case. The advective volume flux is about zero (the 50 m depth over which the fluxes are calculated moves with the free surface), and thus the difference in advective heat flux for these three cases indicates that significantly warmer water is advected into the sound during summer when the Ross Sea Polynya is open and that the presence of the iceberg also somewhat reduces the advection of warm water into the Sound. The difference in the total advected heat over the summer of 2002–2003 would lead to a difference in the average temperature of 0.32°C between the CLMICE case and the ICEBERG case, and a difference of only 0.06°C between the VARICE case and the ICEBERG case. In the model the advection of Ross Sea Polynya heat into the area is a significant part of the summer heat budget.

4. Discussion and Conclusions

[36] The scientific literature has competing ideas about the importance of surface winds versus the advection of
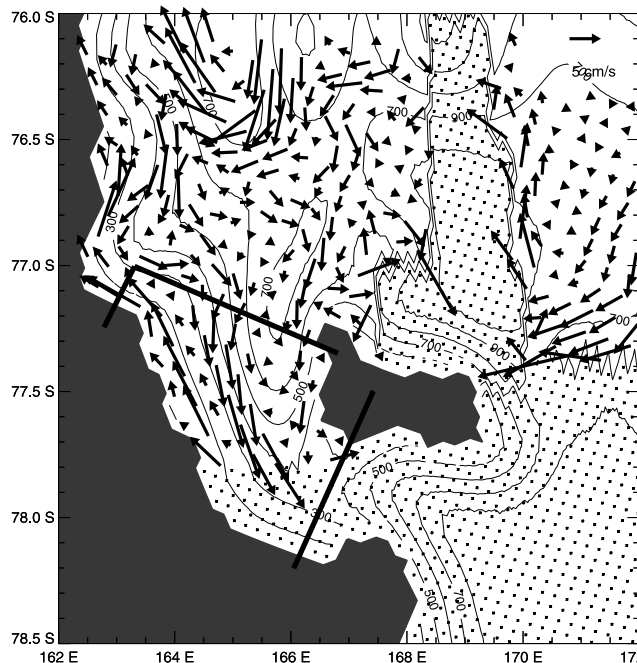

Figure 13. Model circulation at 20 m averaged over January and February for both years for the ICEBERG case.

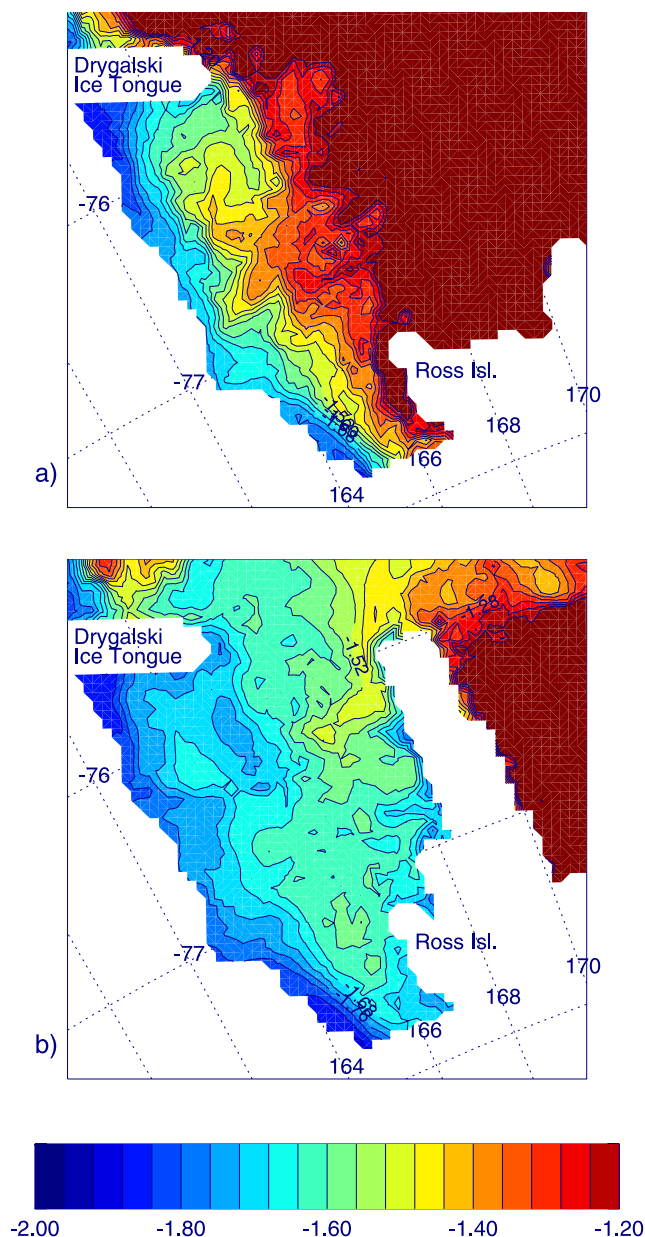**Figure 14.** Model temperature (°C) at 30 m in mid-January 2003 for the (a) CLMICE case and (b) ICEBERG case.

warm water from below in reducing the sea ice concentration in the Ross Sea Polynya. Our model does not have active sea ice, but it produces reasonable SSTs in the polynya so the heat budget is informative. Surface terms are the primary factor in the heat budget, but advective and vertical diffusive terms do indeed play a significant role, lending support to the idea that CDW intrusions are important. A coupled dynamic sea ice, ocean circulation model for the Ross Sea is in development which should be able to give more definitive answers on the relative importance of different surface forcings in the appearance and maintenance of the Ross Sea Polynya.

[37] Simulating the highly variable sea ice conditions in 2001–2003 by imposing them on the model did show several interesting effects that were due to the changing

sea ice. For example, the reduced opening of the Ross Sea Polynya in austral summer 2002–2003 reduced the basal melting over a full year across the entire Ross Ice Shelf by 12% due to the reduction of warm surface waters from the polynya flowing under the shelf.

[38] The highly variable sea ice also had an effect on the creation of high salinity water. An area in the western Ross Sea where HSSW has been observed to form shows an increase in HSSW starting in winter 2002 in the VARICE simulation when compared to the CLMICE case. Some of this increase is due to the ice concentrations in the immediate area. The VARICE simulation had a reduced surface flux of fresh water at several times from September 2001 through April 2002. This relative increase in salinity becomes apparent in the HSSW the following winter when the wintertime convection is strong enough for this signal to affect the deeper water. However, much of the extra salinity in the region in the VARICE case was due to advection from outside the area.

[39] The idea that interannual changes in HSSW formation on the shelf are more a result of remote rather than local processes has been previously suggested. *Jacobs et al.* [2002] reported a "substantial decrease in shelf water salinity" over a 40 a period based on repeated measurements taken north of Ross Island and hypothesized that the likely sources of freshening for the water on the continental shelf were waters imported onto the shelf by the coastal current and from the southern edge of the Ross Gyre. *Assmann and Timmermann* [2005] used a moderate resolution (≈35 km at Ross Island) circumpolar model (BRIOS) to study the variability of dense water formation in the Ross Sea. They suggested that part of the interannual decrease in the salinity found by *Jacobs et al.* [2002] was an aliasing artifact due to undersampling of periodic behavior, but these variations were predominantly due to changes in the salinity and temperature of the inflowing water that originated in the Amundsen and Bellingshausen Seas. *Budillon and Spezie* [2000] used data from three summer cruises in the Terra Nova Bay area to posit that the deep waters in this part of the Ross Sea may be affected more by "variations in the
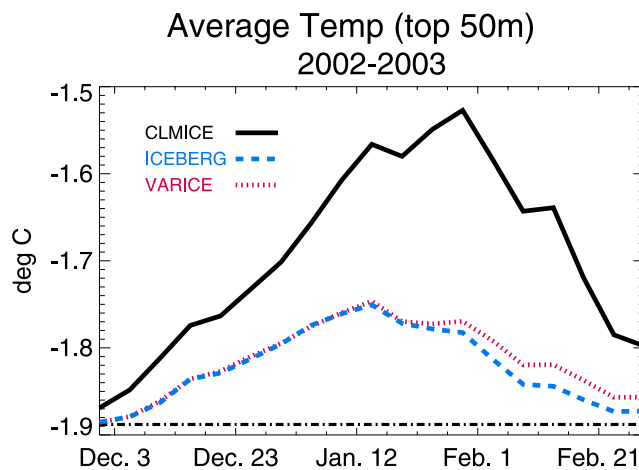

Figure 15. Average temperature (°C) over the top 50 m in McMurdo Sound during summer 2002–2003 for the three simulations. The straight dash-dotted line near the bottom represents the surface freezing point.
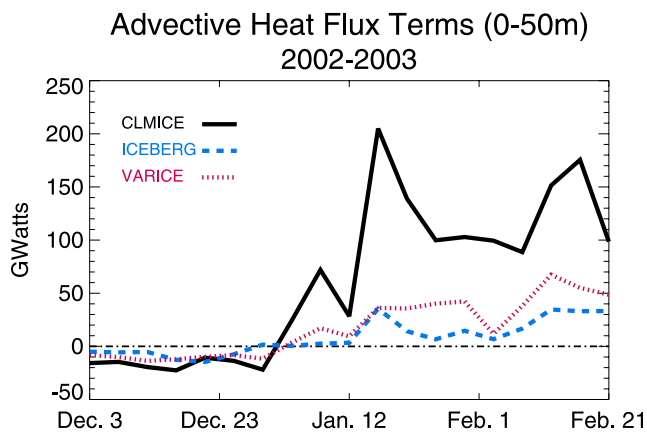
Figure 16. Advective heat flux term over the top 50 m in McMurdo Sound during summer 2002–2003 for the three simulations.

large-scale oceanic current than by local oceanic or atmospheric processes providing a different preconditioning of the water column for the winter vertical convection during the HSSW formation phases.''

[40] During the austral summers of 2001–2002 and 2002–2003, there was unusually extensive sea ice in McMurdo Sound. The fast ice in McMurdo Sound was more extensive than ever recorded, and although the pack ice in the western part of the sound was typical, there was much more pack ice than usual in the eastern part. In a typical year, the annual sea ice begins to form in March or April and continues to thicken until November or December, when it reaches an average thickness of 2 m [*Leventer et al.*, 1987; *Gow et al.*, 1998]. The edge of the fast ice then retreats southward until mid-February when much of the remaining ice breaks out. Measurements show that the fast ice in the western sound does not thin appreciably prior to its breakout [*Mitchell and Bye*, 1985; *Leventer et al.*, 1987]. However, *Leventer et al.* [1987] showed that the fast ice in the eastern part of the sound melted from 1.5 to 0.7 m before breakout. This thinning is thought to be due primarily to bottom melting from relatively warm currents with only minimal melting at the top [*Gow et al.*, 1998]. The difference in heat flux advected into the top 50 m of the eastern half of the McMurdo Sound model box over the summer of 2002–2003 between the CLMICE and ICEBERG cases is enough to melt an average thickness of 24 cm of ice. This decline in basal melt due to B-15A and (primarily) the late opening of the Ross Sea Polynya due to C-19 is significant and would lead to increased strength of the land-fast ice and delayed breakout in summer.

[41] If the smaller Ross Sea Polynya in austral summer 2002–2003 contributed significantly to the ice conditions in McMurdo Sound, then one would expect to see more ice in the Sound (or a later breakout of the fast ice) in early 2003 than in early 2002. This increase appears in the SSM/I data, but at 25-km resolution, it is difficult to have confidence in the values inside McMurdo Sound. Higher resolution (effective resolution of 4 km) sea ice extent images computed from QuikSCAT data [*Redmund and Long*, 1999] on 5 February for several years (Figure 17) show more ice in McMurdo for both of the years (2002 and 2003) when the

icebergs were present than in 2000. However, in 2003, even when the Ross Sea Polynya had finally opened, there was still a great deal of sea ice just west of the icebergs.

[42] Iceberg B-15A had an effect on the circulation, temperature, and salinity in the McMurdo Sound region. While we cannot simulate all possible effects of the iceberg (e.g., advection of pack ice into the sound, changes in the local winds due to the iceberg), the model does show that the iceberg changes the circulation and results in less heat being advected into the sound. However, a bigger effect on the heat advected into the sound was due to iceberg C-19 and its reduction of the size of the Ross Sea Polynya, thus reducing the amount of warm surface water available to advect into the sound. This iceberg may also have restricted the advection of sea ice out of McMurdo Sound, but we cannot simulate that effect with this model.

[43] The extensive sea ice in the Sound disrupted breeding at one of the largest Adélie penguin (*Pygoscelis adeliae*) colonies by making it difficult for the birds to return from their feeding grounds in open water [*Arrigo et al.*, 2002]. Observations in McMurdo Sound also showed that the pteropod *Limacina helicina* was absent for the first time on record [*Seibel and Dierssen*, 2003]. It was hypothesized that its absence was due to either food limitation or changes in local currents caused by the grounding of B-15A that prevented the phytoplankton bloom and associated pteropod populations from being advected into McMurdo Sound from the open waters of the Ross Sea. While the temperature changes shown by the model are not great enough to
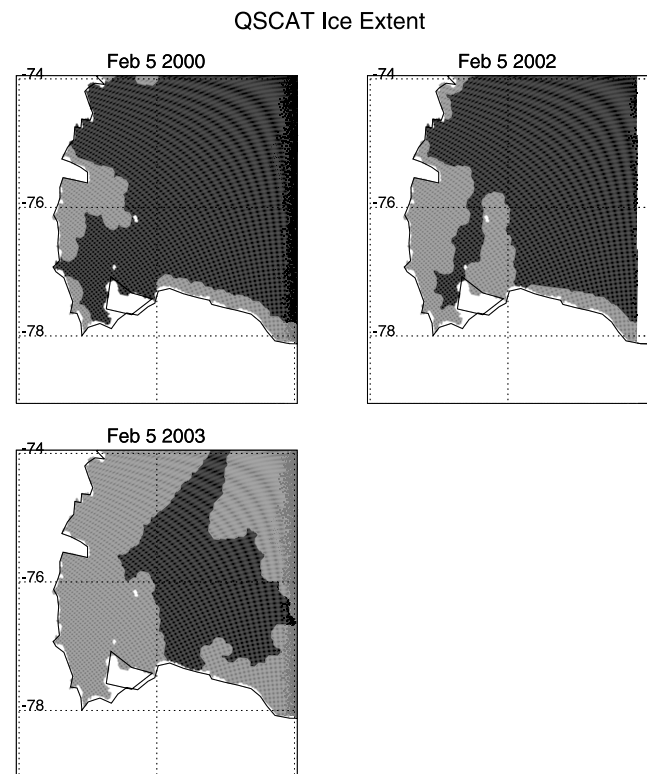

Figure 17. Sea ice extent from QuikSCAT for the southwest Ross Sea on 5 February 2000 (pre-B15A), 2002, and 2003. The sea ice edge here is comparable to the 30% ice concentration for SSM/I data.

influence biological processes significantly, changes in the concentration and distribution of ice directly impact phytoplankton growth via irradiance limitation (ice and snow cover reduce in situ irradiance by up to 99% of surface photon fluxes). We speculate that the icebergs also reduced the area's phytoplankton growth and biomass by reducing advective input of organic matter from the Ross Sea proper. Such reductions could influence the entire ecosystem and ultimately result in unpredictable changes to the food web. Despite suggestions of such changes [*Seibel and Dierssen*, 2003], no clear food web manifestations have yet been demonstrated, although physical disruption of migration patterns of megafauna have been observed [*Arrigo et al.*, 2002].

References

Antoine, D., J. Andre, and A. Morel (1996), Oceanic primary productions: 2. Estimations at global scale from satellite (coastal zone color scanner) chlorophyll, *Global Biogeochem. Cycles*, 10, 57–69.

Arrigo, K. R., and G. L. van Dijken (2003), Impact of iceberg C-19 on Ross Sea primary production, *Geophys. Res. Lett.*, 30(16), 1836, doi:10.1029/2003GL017721.

Arrigo, K. R., G. L. van Dijken, D. G. Ainley, M. A. Fahnestock, and T. Markus (2002), Ecological impact of a large Antarctic iceberg, *Geophys. Res. Lett.*, 29(7), 1104, doi:10.1029/2001GL014160.

Assmann, K. M., and R. Timmermann (2005), Variability of dense water formation in the Ross Sea, *Ocean Dyn.*, 55, 68–87.

Barry, J. P., and P. K. Dayton (1988), Current patterns in McMurdo Sound, Antarctica and their relationship to local biotic communities, *Polar Biol.*, 8, 367–376.

Beckmann, A., H. H. Hellmer, and R. Timmermann (1999), A numerical model of the Weddell Sea: Large-scale circulation and water mass distribution, *J. Geophys. Res.*, 104, 23,375–23,391.

Blankenship, D. D., D. L. Morse, J. W. Holt, M. E. Peters, and S. D. Kempf (2002), An airborne radioglaciological survey of iceberg B15a on November 23, 2001, *Eos Trans. AGU*, 83(47), Fall Meet. Suppl., Abstract C52B-01.

Bromwich, D., Z. Liu, A. N. Rogers, and M. L. Van Woert (1998), Winter atmospheric forcing of the Ross Sea polynya, in *Ocean, Ice and Atmosphere Interactions at the Continental Margin*, *Ant. Res. Ser.*, vol. 75, edited by S. S. Jacobs and R. F. Weiss, pp. 101–133, AGU, Washington, D.C.

Budillon, G., and G. Spezie (2000), Thermohaline structure and variability in the Terra Nova Bay polynya, Ross Sea, *Ant. Sci.*, 12, 493–508.

Budillon, G., G. Fusco, and G. Spezie (2000), A study of surface heat fluxes in the Ross Sea (Antarctica), *Ant. Sci.*, 12, 243–254.

Carmack, E. C. (1977), Water characteristics of the Southern Ocean south of the Polar Front, in *A Voyage of Discovery, G. Deacon 70th Anniversary, Supplement to Deep-Sea Research*, edited by M. Angel, pp. 15–42, Pergamon, Elmsford, N. Y.

Casey, K. S., and P. Cornillon (1999), A comparison of satellite and in situ based sea surface temperature climatologies, *J. Clim.*, 12, 1848–1863.

Dinniman, M. S., J. M. Klinck, and W. O. Smith Jr. (2003), Cross-shelf exchange in a model of the Ross Sea circulation and biogeochemistry, *Deep Sea Res. II*, 50, 3103–3120.

Fairall, C. W., E. F. Bradley, D. P. Rogers, J. B. Edson, and G. S. Young (1996), Bulk parameterization of air-sea fluxes for Tropical Ocean-Global Atmosphere Coupled-Ocean Atmosphere Response Experiment, *J. Geophys. Res.*, 101, 3747–3764.

Fichefet, T., and H. Goosse (1999), A numerical investigation of the spring Ross Sea polynya, *Geophys. Res. Lett.*, 26, 1015–1018.

Foldvik, A., and T. Kvinge (1974), Conditional instability of sea water at the freezing point, *Deep Sea Res.*, 21, 229–243.

Gloersen, P., W. J. Campbell, D. J. Cavalieri, J. C. Comiso, C. L. Parkinson, and H. J. Zwally (1992), Arctic and Antarctic sea ice, 1978–1987: Satellite passive-microwave observations and analysis, *NASA Spec. Publ.*, SP-511, 290 pp.

Gordon, A. L., E. Zambianchi, A. Orsi, M. Visbeck, C. F. Guilivi, T. Whitworth III, and G. Spezie (2004), Energetic plumes over the western Ross Sea continental slope, *Geophys. Res. Lett.*, 31, L21302, doi:10.1029/2004GL020785.

Gow, A. J., S. F. Ackley, J. W. Govoni, and W. F. Weeks (1998), Physical and structural properties of land-fast sea ice in McMurdo Sound, Antarctica, in *Antarctic Sea Ice: Physical Processes, Interactions and Variability*, *Ant. Res. Ser.*, vol. 74, edited by M. O. Jeffries, pp. 355–374, AGU, Washington, D.C.

Grosfeld, K., R. Gerdes, and J. Determann (1997), Thermohaline circulation and interaction between ice shelf cavities and the adjacent open ocean, *J. Geophys. Res.*, 102, 15,595–15,610.

Hall, A., and M. Visbeck (2002), Synchronous variability in the Southern Hemisphere atmosphere, sea ice, and ocean resulting from the annular mode, *J. Clim.*, 15, 3043–3057.

Heath, R. A. (1977), Circulation across the ice shelf edge in McMurdo Sound, Antarctica, in *Polar Oceans*, edited by M. J. Dunbar, pp. 129–149, Arctic Inst. North Am., Calgary.

Hellmer, H. H., and D. Olbers (1989), A two-dimensional model for the thermohaline circulation under an ice shelf, *Ant Sci.*, 1, 325–336.

Hellmer, H. H., S. S. Jacobs, and A. Jenkins (1998), Oceanic erosion of a floating Antarctic glacier in the Amundsen Sea, in *Ocean, Ice and Atmosphere Interactions at the Continental Margin*, *Ant. Res. Ser.*, vol. 75, edited by S. S. Jacobs and R. F. Weiss, pp. 83–99, AGU, Washington, D.C.

Holland, D. M., and A. Jenkins (1999), Modeling thermodynamic ice-ocean interactions at the base of an ice shelf, *J. Phys. Oceanogr.*, 29, 1787–1800.

Holland, D. M., S. S. Jacobs, and A. Jenkins (2003), Modelling the ocean circulation beneath the Ross Ice Shelf, *Ant. Sci.*, 15, 13–23, doi:10.1017/S0954102003001019.

Jacobs, S. S., and J. C. Comiso (1989), Sea ice processes on the Ross Sea Continental Shelf, *J. Geophs. Res.*, 94, 18,195–18,211.

Jacobs, S. S., and C. F. Giulivi (1998), Interannual ocean and sea ice variability in the Ross Sea, in *Ocean, Ice and Atmosphere Interactions at the Continental Margin*, *Ant. Res. Ser.*, vol. 75, edited by S. S. Jacobs and R. F. Weiss, pp. 135–150, AGU, Washington, D.C.

Jacobs, S. S., and C. F. Giulivi (1999), Thermohaline data and ocean circulation on the Ross Sea continental shelf, in *Oceanography of the Ross Sea, Antarctica*, edited by G. Spezie and G. M. R. Manzella, pp. 3–16, Springer, Milan.

Jacobs, S. S., R. G. Fairbanks, and Y. Horibe (1985), Origin and evolution of water masses near the Antarctic continental margin: evidence from $H_2{}^{18}O/H_2{}^{16}O$ ratios in seawater, in *Oceanology of the Antarctic Shelf*, *Ant. Res. Ser.*, vol. 43, edited by S. S. Jacobs, pp. 59–95, AGU, Washington, D.C.

Jacobs, S. S., H. H. Hellmer, C. S. M. Doake, A. Jenkins, and R. M. Frolich (1992), Melting of ice shelves and the mass balance of Antarctica, *J. Glaciol.*, 38, 375–387.

Jacobs, S. S., C. F. Giulivi, and P. A. Mele (2002), Freshening of the Ross Sea during the late 20th century, *Science*, 297, 386–389.

Jenkins, A., H. H. Hellmer, and D. M. Holland (2001), The role of meltwater advection in the formulation of conservative boundary conditions at an ice-ocean interface, *J. Phys. Oceanogr.*, 31, 285–296.

Large, W. G., J. C. McWilliams, and S. C. Doney (1994), Oceanic vertical mixing: A review and model with a nonlocal boundary layer parameterization, *Rev. Geophys.*, 32, 363–403.

Leventer, A., R. B. Dunbar, M. R. Allen, and R. Y. Wayper (1987), Ice thickness in McMurdo Sound, Antarctica, *Ant. J. U.S.*, 22, 94–96.

Lewis, E. L., and R. G. Perkin (1985), The winter oceanography of McMurdo Sound, in *Oceanology of the Antarctic Shelf*, *Ant. Res. Ser.*, vol. 43, edited by S. S. Jacobs, pp. 145–165, AGU, Washington, D.C.

Lingle, C. S., D. H. Schilling, J. L. Fastook, W. S. B. Paterson, and T. J. Brown (1991), A flow band model of the Ross Ice Shelf. Antarctica - response to CO_2-induced climatic warming, *J. Geophys. Res.*, 96, 6849–6871.

Lythe, M. B., D. G. Vaughan, and the BEDMAP Consortium (2001), BEDMAP: A new ice thickness and subglacial topographic model of Antarctica, *J. Geophys. Res.*, 106, 11,335–11,351.

Manzella, G. M. R., R. Meloni, and P. Picco (1999), Current, temperature and salinity observations in the Terra Nova Bay Polynya Area, in *Oceanography of the Ross Sea, Antarctica*, edited by G. Spezie and G. M. R. Manzella, pp. 165–173, Springer, Milan.

Markus, T. (1999), Results from an ECMWF-SSM/I forced mixed layer model of the Southern Ocean, *J. Geophys. Res.*, 104, 15,603–15,620.

Milliff, R. F., J. Morzel, D. B. Chelton, and M. H. Freilich (2004), Wind stress curl and wind stress divergence biases from rain effects on QSCAT surface wind retrievals, *J. Atmos. Oceanic Technol.*, *21*, 1216–1231.

Mitchell, W. M., and J. A. T. Bye (1985), Observations in the boundary layer under the sea ice in McMurdo Sound, in *Oceanology of the Antarctic Shelf*, *Ant. Res. Ser.*, vol. 43, edited by S. S. Jacobs, pp. 167–176, AGU, Washington, D.C.

National Geophysical Data Center (NGDC) (1988), Data Announcement 88-MGG-02, Digital relief of the surface of the Earth, NOAA, Natl. Geophys. Data Cent., Boulder, Colo.

Orsi, A., G. Johnson, and J. Bullister (1999), Circulation, mixing, and production of Antarctic Bottom Water, *Progr. Oceanogr.*, *43*, 55–109.

Peloquin, J. A., and W. O. Smith Jr. (2007), Phytoplankton blooms in the Ross Sea, Antarctica: Interannual variability in magnitude, temporal patterns and composition, *J. Geophys. Res.*, *112*, C08013, doi:10.1029/2006JC003816.

Podestá, G. P., M. Arbelo, R. Evans, K. Kilpatrick, V. Halliwell, and J. Brown (2003), Errors in high-latitude SSTs and other geophysical products linked to NOAA-14 AVHRR channel 4 problems, *Geophys. Res. Lett.*, *30*(11), 1548, doi:10.1029/2003GL017178.

Redmund, Q. P., and D. G. Long (1999), Sea ice extent mapping using Ku-band scatterometer data, *J. Geophys. Res.*, *104*, 11,515–11,527.

Seibel, B. A., and H. M. Dierssen (2003), Cascading trophic impacts of reduced biomass in the Ross Sea, Antarctica: Just the tip of the iceberg?, *Biol Bull.*, *205*, 93–97.

Shabtaie, S., and C. R. Bentley (1987), West Antarctic ice streams draining into the Ross Ice Shelf: Configuration and mass balance, *J. Geophys. Res.*, *92*, 1311–1336.

Shchepetkin, A. F., and J. C. McWilliams (2003), A method for computing horizontal pressure-gradient force in an oceanic model with a nonaligned vertical coordinate, *J. Geophys. Res.*, *108*(C3), 3090, doi:10.1029/2001JC001047.

Shchepetkin, A. F., and J. C. McWilliams (2005), The regional oceanic modeling system (ROMS): A split-explicit, free-surface, topography-following-coordinate oceanic model, *Ocean Model.*, *9*, 347–404.

Smith, W. H., and D. T. Sandwell (1997), Global sea floor topography from satellite altimetry and ship depth soundings, *Science*, *277*, 1956–1962.

Smith, W. O., Jr., A. R. Shields, J. A. Peloquin, G. Catalano, S. Tozzi, M. S. Dinniman, and V. A. Asper (2006), Interannual variations in nutrients, net community production, and biogeochemical cycles in the Ross Sea, *Deep Sea Res. II*, *53*, 815–833.

Stover, C. L. (2006), A new account of Ross Sea waters: Characteristics, volumetrics, and variability, M.S. thesis, 100 pp., Texas A&M Univ., College Station, Tex.

Timmermann, R., A. Beckmann, and H. H. Hellmer (2002), Simulations of ice-ocean dynamics in the Weddell Sea: 1. Model configuration and validation, *J. Geophys. Res.*, *107*(C3), 3024, doi:10.1029/2000JC000741.

VanWoert, M. L. (1999), Wintertime dynamics of the Terra Nova Bay polynya, *J. Geophys. Res.*, *104*, 7753–7769.

Vaughan, D. G., G. J. Marshall, W. M. Connolley, C. Parkinson, R. Mulvaney, D. A. Hodgson, J. C. King, C. J. Pudsey, and J. Turner (2003), Recent rapid regional climate warming on the Antarctic Peninsula, *Clim. Change*, *60*, 243–274.

White, W. B., and R. G. Peterson (1996), An Antarctic circumpolar wave in surface pressure, wind, temperature and sea-ice extent, *Nature*, *380*, 699–702.

Wilkin, J., and K. S. Hedström (1998), User's manual for an orthogonal curvilinear grid-generation package, *Tech. Rep.*, 33 pp., Inst. of Mar. and Coastal Sci., Rutgers Univ., New Brunswick, N. J.

Yuan, X., and D. G. Martinson (2000), Antarctic sea ice extent variability and its global connectivity, *J. Clim.*, *13*, 1697–1717.

Zillman, J. W. (1972), A study of some aspects of the radiation and the heat budgets of the southern hemisphere oceans, *Meteorolgical Studies*, vol. 26, 562 pp., Bur. of Meteorol., Dept. of the Int., Canberra, ACT, Australia.

Zwally, H. J., J. C. Comiso, and A. L. Gordon (1985), Antarctic offshore leads and polynyas and oceanographic effects, in *Oceanology of the Antarctic Shelf*, *Ant. Res. Ser.*, vol. 43, edited by S. S. Jacobs, pp. 203–226, AGU, Washington, D. C.

————————————

M. S. Dinniman and J. M. Klinck, Center for Coastal Physical Oceanography, Old Dominion University, 4111 Monarch Way, Norfolk, VA 23508, USA. (msd@ccpo.odu.edu)

W. O. Smith Jr., Virginia Institute of Marine Science, College of William and Mary, Gloucester Point, VA 23062, USA.